Clinical Radiology 74 (2019) 287–294

Contents lists available at ScienceDirect

Clinical Radiology

journal homepage: www.clinicalradiologyonline.net

Can quantitative CT texture analysis be used to differentiate subtypes of renal cell carcinoma?

G.-M.-Y. Zhang [a], B. Shi [b], H.-D. Xue [a], B. Ganeshan [c], H. Sun [a,*], Z.-Y. Jin [a,**]

[a] *Department of Radiology, Peking Union Medical College Hospital, Peking Union Medical College, Chinese Academy of Medical Sciences, Beijing, China*

[b] *Department of Radiology, Shenzhen Sun Yat-Sen Cardiovascular Hospital, No. 1021 Dongmen Road North, Luohu District, Shenzhen 518001, China*

[c] *Feedback Plc, Cambridge, England, UK*

ARTICLE INFORMATION

Article history:
Received 27 March 2018
Accepted 23 November 2018

AIM: To investigate whether computed tomography (CT) texture analysis (TA) can be used to differentiate non-clear-cell renal cell carcinoma (non-ccRCC) from clear-cell RCC (ccRCC) and classify non-ccRCC subtypes.

MATERIALS AND METHODS: One hundred ccRCC and 27 non-ccRCC (12 papillary and 15 chromophobe) were analysed. Texture parameters quantified from multiphasic CT images were compared for the objectives. Receiver operating characteristic (ROC) analysis was performed and the area under the ROC curve (AUC) was calculated. The optimal discriminative texture parameters were used to produce support vector machine (SVM) classifiers. Diagnostic accuracy and 10-fold cross-validation was performed.

RESULTS: Compared to ccRCC, non-ccRCC had significantly lower mean grey-level intensity (mean), standard deviation (SD), entropy, mean of positive pixels (MPP), and higher kurtosis ($p<0.001$). A model incorporating SD, entropy, MPP, and kurtosis produced an AUC of 0.94±0.03 with an accuracy of 87% (sensitivity=89%, specificity=92%) to identify non-ccRCC from ccRCC. Compared to chromophobe RCC, papillary RCC had significantly lower mean and MPP ($p=0.002$). A model incorporating SD, MPP, and skewness resulted in an AUC of 0.96±0.04 with an accuracy of 78% (sensitivity=87%, specificity=92%) to differentiate between papillary and chromophobe RCC.

CONCLUSION: CT TA could potentially be used as a less invasive tool to classify histological subtypes of RCC.

© 2018 The Royal College of Radiologists. Published by Elsevier Ltd. All rights reserved.

Introduction

Renal cell carcinoma (RCC) is a common malignancy with an increasing mortality rate.[1,2] It is a heterogeneous disease with different histological subtypes. Clear cell, papillary, and chromophobe RCC are the most common subtypes.[2] The histological classification of RCC is important as clear-cell RCC (ccRCC) generally has a worse prognosis compared to

* Guarantor and correspondent: H. Sun, Tel.: +86 13146802900; Fax: +86 69255442.

** Guarantor and correspondent: Z. Jin, Tel.: +86 13601037675; Fax: +86 69255442.

E-mail addresses: zhang_stacey@outlook.com (G.-M.-Y. Zhang), dearicy@yahoo.com (B. Shi), bjdanna@163.com (H.-D. Xue), balaji@texrad.co.uk (B. Ganeshan), sunhao_robert@126.com (H. Sun), zhengyu_jin@126.com (Z.-Y. Jin).

https://doi.org/10.1016/j.crad.2018.11.009
0009-9260/© 2018 The Royal College of Radiologists. Published by Elsevier Ltd. All rights reserved.

other subtypes.[3,4] As the available targeted agents of metastatic RCC (mRCC) mainly relate to ccRCC,[5–7] the optimal treatment for mRCC with non-clear cell histology is still under investigation. A tumour biopsy is indicated to provide histological information before commencing systemic treatment, but its invasive nature and unsatisfactory accuracy have limited its clinical application in certain patients.[8] It would be helpful if there was a safer and much less invasive method to characterise RCC subtypes.

Previous studies have focused on the use of enhancement of lesions at multiphasic computed tomography (CT) or magnetic resonance imaging (MRI) to differentiate ccRCC from papillary RCC (pRCC) or chromophobe RCC (chRCC),[9–12] but it is still challenging to diagnose the RCC subtype correctly as the interpretation of imaging findings is a subjective process and an accurate prediction of histological RCC subtype strongly depends on the experience and expertise of the radiologist. In addition, due to lack of validation on a larger scale, clinical application of these methods is limited. A more objective method is required to improve diagnosis of RCC subtype.

Texture analysis (TA) is an emerging imaging tool to quantify tissue heterogeneity that may not be perceived by the naked eye. It involves an objective computer-aided measurement of grey-level patterns within the lesions. A few studies have reported that TA could differentiate renal fat-poor angiomyolipoma from RCC accurately[13–16]; however, whether TA could discriminate RCC subtypes has been controversial. Raman *et al.*[16] and Yan L *et al.*[13] demonstrated that CT TA could differentiate ccRCC from pRCC, but Hodgdon *et al.*[14] showed there was no difference between ccRCC, pRCC, and chRCC on unenhanced CT images. Further studies are needed to investigate the potential value of CT TA in characterising RCC subtypes. As stated earlier that non-clear cell RCC (non-ccRCC) is not recommended for targeted therapies, discriminating non-ccRCC from ccRCC is far more clinically relevant, which could help patients with non-ccRCC avoid possible side effects and enormous cost of targeted agents. To the authors' knowledge, the potential of CT TA has not been explored in this context of differentiating non-ccRCC from ccRCC.

The primary aim of this study was to evaluate the diagnostic performance of CT TA retrospectively to differentiate non-ccRCC from ccRCC, and a secondary aim was to investigate whether CT TA could differentiate non-ccRCC subtypes of pRCC and chRCC on multiphasic images.

Materials and methods

Patient selection

The institutional review board approved this retrospective study and waived the requirement for informed consent. Between June 2014 to August 2015, 165 patients with a diagnosis of RCC confirmed histologically on entire tumour resection were identified. Twenty-nine patients were excluded for absence of preoperative multiphasic CT images in the picture archiving and communication system (PACS), including 24 patients with ccRCC, three patients with pRCC, and two patients with chRCC. Two radiologists with 10 and 13 years of experience in abdominal imaging reviewed all the images and excluded another 10 patients with ccRCC in whom there was almost no solid component in the lesions for TA. The final study population comprised 126 patients and the details are provided in Fig 1.

CT examination

All the patients underwent a preoperative three-phasic abdominal CT examination (Somatom Definition Flash; Siemens Healthcare, Forchheim, Germany). Protocol details are provided in Table 1. After the unenhanced scan, intravenous injection of 100 ml contrast material (Ultravist 370, Bayer ScheringPharma AG, Germany) followed by a 100 ml saline chaser were administered at a rate of 4 ml/s. A bolus-tracking algorithm (CareBolus, Siemens Medical Solutions) was used and a region of interest (ROI) was placed in the thoraco-abdominal aorta junction. The corticomedullary phase was initiated 5 seconds after the bolus-triggering threshold of 120 HU was reached and the nephrographic phase occurred 50 seconds after the corticomedullary imaging acquisition.

CT TA

All the images were de-identified before being accessed by the researchers. Two radiologists with 10 and 13 years of experience in abdominal imaging reviewed all the images and disagreement was resolved in consensus. Both reviewers were blinded to clinical and histological information. For each lesion in each phase, only one axial image with the optimal representation of the largest cross-sectional tumour area was chosen for TA. One of the two reviewers measured the maximal diameter of each lesion on the selected axial images and repeated the measurement

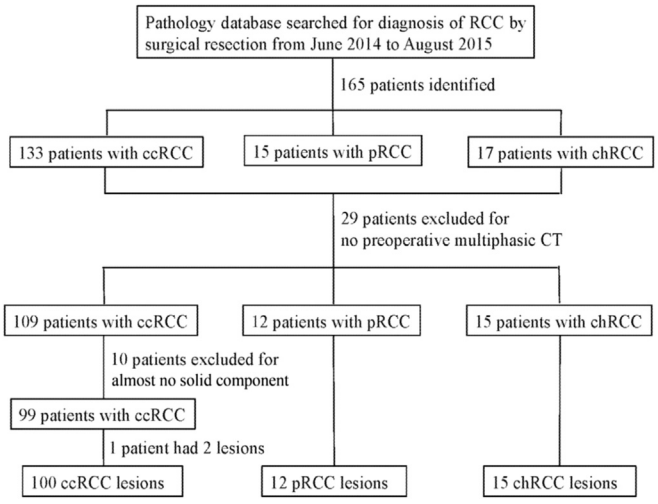

Figure 1 Flowchart of patient population and exclusion criteria. ccRCC, clear cell RCC; non-ccRCC, non-clear cell RCC; pRCC, papillary RCC; chRCC, chromophobe RCC.

Table 1
Imaging parameters of the computed tomography examination.

Parameter	
Tube potential, kV	120
Tube current, mAs	Variable tube current with automatic tube-current modulation activated
Pitch	0.9
Gantry rotation time, second	0.28
Collimation, mm	128×0.6
Kernel	B30f (medium smooth)
Acquisition slice thickness, mm	5
Field of view, mm	300

several months later to assess the intra-observer agreement. Another radiologist also measured the maximal diameter of each lesion to assess the inter-observer agreement. All the selected images were exported from PACS and uploaded to the TexRAD commercial research software (TexRAD Ltd, www.texrad.com, part of Feedback Plc, Cambridge, UK). A single trained operator carried out all the TA and repeated the process 8-weeks later. The average value of two measurements for each texture parameter was calculated and recorded.

For each lesion, a ROI was manually delineated slightly within the lesion border leaving an approximate distance of 1–2 mm from the outline in order to minimise volume averaging from surrounding perirenal fat or normal renal parenchyma. Confounding factors such as air, dense calcification, and necrosis without enhancement were excluded when drawing the ROIs to minimise their impact on the CT TA (Fig 2a). Furthermore, the CT TA algorithm setting excluded pixels with values less than −50 and >200 HU from inclusion in the texture analysis to increase the robustness in the quantification. As the outline of lesions could be difficult to define on unenhanced images, the corresponding matched enhanced images of each lesion were referenced during delineation. ROIs for each axial section for matched unenhanced, corticomedullary and nephrographic CT images were then used for TA.

TA comprised a two-step process that involved selective scale image filtration to extract features of different sizes followed by texture quantification by histogram analysis. Image filtration utilised a Laplacian of Gaussian spatial bandpass filter to produce a series of derived images highlighting features at different spatial scales. The size of the image features highlighted by the filter is denoted by the spatial scaling factor (SSF), which ranges between object radii of 0, 2, 3, 4, 5, and 6 mm. SSF can be considered as the width at which structures in the image will be highlighted while structures less than this width will become blurred. SSF 0 indicates used of no filtration (used as control), 2 indicates fine, 3–5 indicates medium, and 6 indicates coarse texture scales, respectively (Fig 2b–d). Six texture parameters were derived from histogram analysis: mean grey-level intensity (mean, brightness), standard deviation (SD, degree of variation from the mean), entropy (irregularity of pixel intensity), mean of positive pixels (MPP), skewness (symmetry of the histogram distribution), and kurtosis (sharpness of the histogram distribution).[17] For each lesion in each phase, all the six parameters across each SSF were recorded.

Statistical analysis

Intra- and interobserver agreement were calculated for the measurement of the maximum diameter of the lesions by using the intraclass correlation coefficient (ICC) test (0.00–0.20, poor agreement; 0.21–0.40, fair agreement; 0.41–0.60, moderate agreement; 0.61–0.80, good agreement; 0.81–1.00, excellent agreement). Papillary RCC and chRCC were classified together as non-ccRCC. Mann–Whitney *U*-tests were used to compare the value of each texture parameter in each phase for the research purposes (SPSS for Mac, version 20, SPSS, Chicago, IL, USA). Although a two-sided $p<0.05$ indicated a significant difference, to control for type I errors arising from multiple comparisons, the individual significance level was adjusted as proposed by Cross and Chaffin[18]:

$$p^{*}=p\times[k-x+1]^{-1}$$

where p^{*} is the adjusted significance level for an individual test, p is the nominal significance level for the sequence of tests, k is the total number of the tests, and x is the number of significant tests. Receiver operating characteristic (ROC) curves and the area under the ROC curves (AUC) were calculated for each texture parameter in each phase and Pearson's correlation coefficient (r) between texture features at each SSF in each phase was evaluated so that only one of the features that showed a high correlation ($r>0.90$) was selected to build the classifiers. As an AUC of ≥0.8 generally indicates a good test, all the texture features with an AUC of ≥0.8 were selected as predictors. In cases where all the AUCs were <0.8, only three texture parameters with the top three AUC values were selected as predictors to minimise the likelihood of overfitting. Combinations of predictors were used to train multiple support vector machine (SVM) classifiers, and ROC curves were computed by the predicted values of regression of SVM for each SSF in each phase to determine the optimal combination. An SVM with a nonlinear radial basis function kernel was implemented in the "SVM" function in R Package "e1071" (Version 1.6–7, R Software), using the Library for Support Vector Machines (or LIBSVM) library.[19] The stability of classification was evaluated through 10-fold cross-validation.

Results

General characteristics of the 126 patients with 127 RCC lesions (100 ccRCC, 12 pRCC, 15 chRCC) are summarised in Table 2. The mean time from preoperative CT evaluation to nephrectomy was 20 days for all RCC (range, 0–35 days). For the measurement of maximum diameter of the lesions, excellent intra-observer (intraclass correlation coefficient, ICC=0.95) and interobserver agreement (ICC=0.91) were found. The average size of all the RCC was 4.9±2.6 cm. There

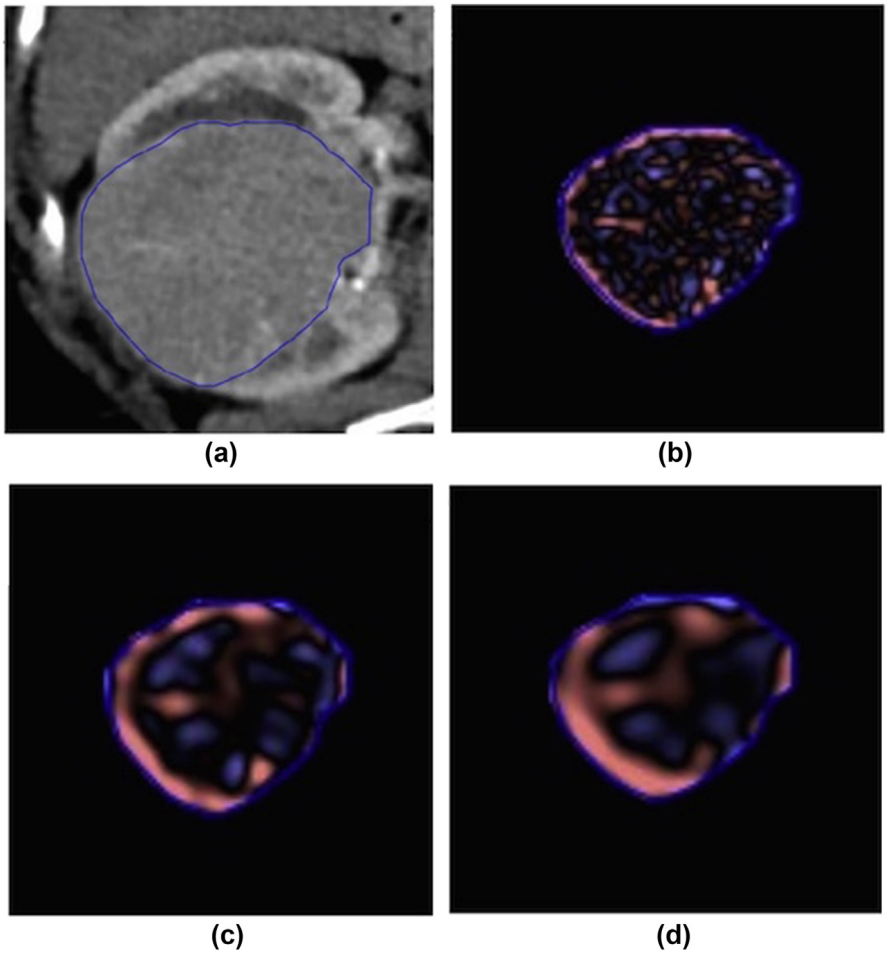

Figure 2 Demonstration of ROI delineation within the lesion and corresponding texture images of different texture scales. Corticomedullary CT image in a patient with a right renal lesion shows a region of interest (blue contour) drawn within the border of the lesion (a). Corresponding texture analysis images display fine (b), medium (c), and coarse (d) textures obtained by using SSF 2, 4, and 6, respectively.

was no significant difference in the average size of lesions among ccRCC (4.5±2.1), pRCC (6.5±3.7), and chRCC (6.1±3.2; $p>0.05$).

Table 2
Characteristics of patients and renal cell carcinomas.

Characteristic	All	ccRCC	non-ccRCC		
			All	pRCC	chRCC
Sex[a]					
Male	83(66)	66(67)	17(63)	10(83)	7(47)
Female	43(34)	33(33)	10(37)	2(17)	8(53)
Age (years)[b]	54±12	55±12	51±15	53±18	49±13
Side					
Left	66(52)	55(55)	11(41)	5(42)	6(40)
Right	61(48)	45(45)	16(59)	7(58)	9(60)

Data are numbers of lesions and data in parentheses are percentage, unless otherwise indicated.
RCC, renal cell carcinoma; ccRCC, clear-cell RCC; non-ccRCC, non-clear-cell RCC; pRCC, papillary RCC; chRCC, chromophobe RCC.
[a] Data are numbers of patients. There was no significant difference in the portion of male patients among ccRCC, pRCC, and chRCC groups ($p>0.05$).
[b] Data are mean ± standard deviation. There was no significant difference in mean age among ccRCC, pRCC, and chRCC groups ($p>0.05$).

Differentiating non-ccRCC from ccRCC

The median and interquartile range (IQR) associated with each texture parameter, the corresponding p, and the AUC values for assessing the difference between non-ccRCC and ccRCC are provided in Electronic Supplementary Material Table S1. Compared to ccRCC, all the six texture parameters quantified from unenhanced images and skewness quantified from enhanced images did not show any significant differences from non-ccRCC ($p>0.001$ after Cross and Chaffin correction); however, on enhanced images, kurtosis was significantly higher while mean, SD, entropy, and MPP were significantly lower at all the texture scales (SSF 0–6) in non-ccRCC ($p<0.001$ after Cross and Chaffin correction). As Mean and MPP quantified from SSF0 on both unenhanced and enhanced images, SD and entropy quantified from SSF2 on enhanced images, SD and MPP quantified from SSF2–5 on enhanced images all had a Pearson's correlation coefficient >0.90, only one of these correlated features at each SSF in each phase was selected to build the classifiers.

Regression models produced by combining the optimal discriminative texture features are summarised in Table 3. To identify non-ccRCC from ccRCC, all the models resulted

Table 3
ROC curves for combinations of texture features for differentiating non-clear-cell renal cell carcinoma from clear-cell renal cell carcinoma.

Phase	SSF	Model	AUC[a]	*p*-Value	SVM[b]	Sensitivity	Specificity
UE	0	MPP+ skewness+ kurtosis[c]	0.82±0.05	<0.001	79	0.78	0.86
	2	Mean+ skewness+ kurtosis	0.79±0.06	<0.001	79	0.79	0.86
	3	Mean+ MPP+ kurtosis	0.73±0.06	<0.001	80	0.59	0.85
	4	MPP+ skewness+ kurtosis	0.80±0.06	<0.001	80	0.74	0.83
	5	Entropy+ MPP+ kurtosis	0.74±0.06	<0.001	76	0.59	0.84
	6	Entropy+ MPP+ kurtosis	0.76±0.06	<0.001	76	0.63	0.88
CM	0	Entropy+ MPP+ kurtosis	0.92±0.04	<0.001	86	0.85	0.88
	2	Mean+ entropy+ MPP	0.92±0.03	<0.001	87	0.89	0.90
	3	Entropy+ MPP+ kurtosis	0.93±0.03	<0.001	88	0.96	0.85
	4	Entropy+ MPP+ kurtosis	0.92±0.03	<0.001	87	0.89	0.88
	5	Entropy+ MPP+ kurtosis	0.92±0.03	<0.001	88	0.93	0.89
	6	SD+ entropy+ MPP+ kurtosis[c]	0.94±0.03	<0.001	87	0.89	0.92
N	0	Entropy+ MPP+ kurtosis[c]	0.89±0.04	<0.001	85	0.89	0.83
	2	Entropy+ MPP+ kurtosis	0.84±0.05	<0.001	81	0.74	0.89
	3	Entropy+ MPP+ kurtosis	0.83±0.05	<0.001	83	0.74	0.90
	4	Entropy+ MPP+ kurtosis	0.83±0.05	<0.001	87	0.70	0.90
	5	Mean+ entropy+ MPP	0.88±0.04	<0.001	82	0.93	0.78
	6	SD+ entropy+ MPP	0.89±0.03	<0.001	84	0.89	0.81

AUC, area under the receiver operating characteristic (ROC) curve, SSF, spatial scaling factor, SVM, support vector machine, Sen, sensitivity, Spe, specificity, Mean, mean grey-level intensity, SD, standard deviation, MPP, mean of positive pixels, UE, unenhanced, CM, corticomedullary, N, nephrographic.
[a] Data are mean AUC ± standard error.
[b] Accuracy of the SVM classifier after 10-fold cross-validation.
[c] Model with the highest AUC in each phase.

in AUCs >0.7. On unenhanced images, the model incorporating MPP, skewness, and kurtosis at SSF0 produced the highest AUC of 0.82±0.05 (p<0.001) with 78% sensitivity and 86% specificity (Fig 3a). On corticomedullary images, the highest AUC of 0.94±0.03 (p<0.001) was reached at SSF6 by the model incorporating SD, entropy, MPP, and kurtosis with 89% sensitivity and 92% specificity (Fig 3b). On nephrographic images, the model incorporating entropy, MPP, and kurtosis at SSF0 yielded the highest AUC of 0.89±0.04 (p<0.001) with 89% sensitivity and 83% specificity (Fig 3c). The 10-fold cross-validation support vector machine (SVM) accuracy arranged from 76% to 88% for each combination of texture features (Table 3).

Differentiation between pRCC and chRCC

The median and IQR associated with each texture parameter, the corresponding p and AUC values for differentiating between pRCC and chRCC are summarised in Electronic Supplementary Material Table S2. Only mean and MPP quantified from SSF0 on corticomedullary images were significantly different (p=0.002) between the two subtypes. Mean and MPP were both significantly lower in pRCC (mean: median pRCC, 48.2; IQR, 38.1–60.0; median chRCC,72.4; IQR, 54.1–101.5; p=0.02; MPP: median pRCC, 49.6; IQR, 40–61.1; median chRCC, 74.6; IQR, 58.3–101.6; p=0.002). The mean AUC ± standard error associated with Mean (0.84 ± 0.08) and MPP (0.85 ± 0.07) were >0.8. As mean and MPP quantified from SSF0 on both unenhanced and enhanced images, SD and entropy quantified from SSF3–6 on unenhanced images, SD and MPP quantified from SSF2 on enhanced images and SSF3, four on corticomedullary images all had a Pearson's correlation coefficient >0.90, only one of these correlated features at each SSF in each phase was selected to build the classifiers.

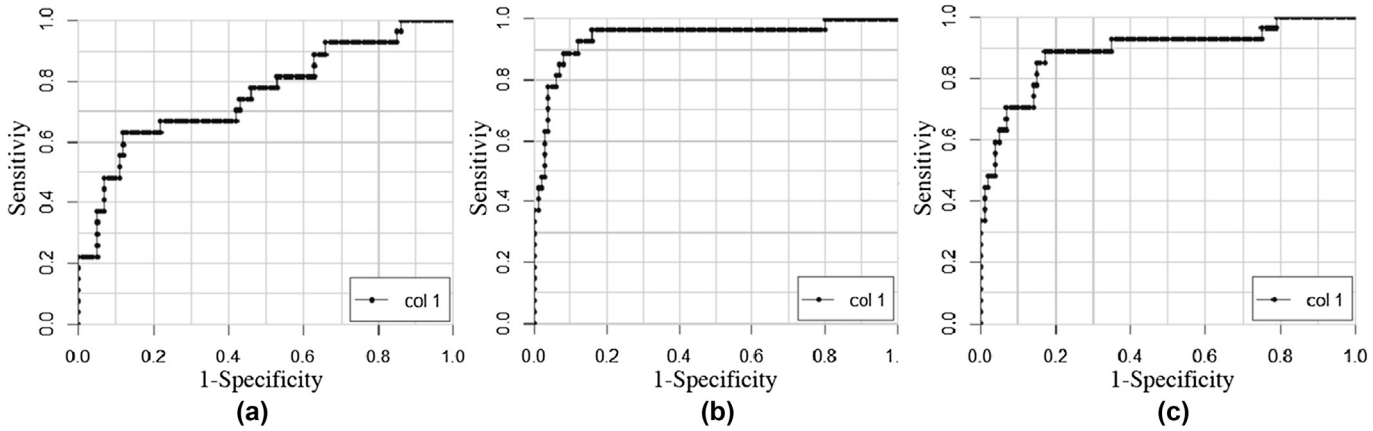

Figure 3 ROC curves for SVM performances with the highest AUC value on (a) unenhanced, (b) corticomedullary, and (c) nephrographic phase images to identify non-ccRCC from ccRCC.

The results of different regression models to differentiate between pRCC and chRCC are summarised in Table 4. On unenhanced images, all the AUCs were significantly >0.7 and the model incorporating entropy, MPP, and kurtosis quantified from SSF6 produced an AUC of 0.84±0.08 (p=0.077) with 67% sensitivity and 100% specificity (Fig 4a). On corticomedullary images at SSF0, SD combined with MPP and skewness yielded an AUC of 0.96±0.04 with 87% sensitivity and 92% specificity (Fig 4b). On nephrographic images, the highest AUC of 0.93±0.05 (p<0.001) with 93% sensitivity and 83% specificity (Fig 4c) was reached at SSF0 by incorporating MPP, skewness, and kurtosis. The 10-fold cross-validation SVM accuracy arranged from 30% to 78% for each combination of texture features (Table 4).

Discussion

The results of the present study show that texture parameters of SD, entropy, and MPP seem to be strong predictors of non-ccRCC, while MPP and skewness are helpful texture features to further differentiate between pRCC and chRCC. The present results indicate that TA may serve as a non-invasive method to identify non-ccRCC and it could potentially help those patients avoid unnecessary drug toxicity and financial burden by predicting histological RCC subtype.

The present results showed that non-ccRCC had significantly lower mean, SD, entropy, MPP, and higher kurtosis compared to ccRCC on enhanced CT images. Specifically, MPP quantified from the coarse texture scale (SSF6) on corticomedullary images seems to be a valuable texture feature, and the combination of SD, entropy, MPP, and kurtosis at SSF6 on corticomedullary images is the strongest classifier for non-ccRCC. Generally, the present results were comparable to previous studies of renal, brain, and lung neoplasms.[20–24] Greater heterogeneity is known to be likely related to higher histological grade of malignancy and poorer prognosis.[5–26] From the present study it can be inferred that heterogeneity between RCC subtypes is likely linked to an increasing number of objects or features highlighted in the filtration step and their mean brightness difference compared to the background of lesions resulting in higher mean, SD, entropy, MPP, and lower kurtosis in ccRCC. Skewness tends to be zero with an increasing number of objects highlighted, which may be a general characteristic of RCC subtypes and hence was not a useful discriminator. The present results were consistent with previous studies reporting that higher entropy and lower degree of texture features related to uniformity are characteristics of ccRCC.[13,14] As ccRCC is generally more aggressive than non-ccRCC, it worth investigating the relationship between the texture characteristics and the prognosis of RCC. As for MPP, it has been correlated negatively with angiogenesis in non-small cell lung cancer.[22] To the authors' knowledge, the present study is the first to show that lower MPP on enhanced CT images may help to identify non-ccRCC, and MPP may be a good parameter in addition to kurtosis in vascular tumours as shown previously in treatment-response studies of metastatic RCC.[27] Given that MPP only considers the average intensity of pixels greater than zero and non-ccRCC tends to be generally hypovascular, lower MPP in non-ccRCC appears to be consistent with hypovascular tumours exhibiting fewer bright areas. Furthermore, amongst non-ccRCC, pRCC tends to be even more hypovascular, which potentially explains the even lower value of MPP in pRCC compared to chRCC. MPP on contrast-enhanced CT images may be positively correlated with the blood supply of RCC, and MPP may be a better marker of treatment response compared to size, density, and perfusion. When the present results were compared to similar studies

Table 4
Receiver operating characteristic (ROC) curves for combinations of texture features for differentiating between pRCC and ccRCC.

Phase	SSF	Model	AUC[a]	p-Value	SVM[b]	Sensitivity	Specificity
UE	0	Entropy+ MPP+ skewness	0.76±0.10	0.025	41	0.53	0.92
	2	SD+ entropy+ skewness	0.83±0.08	0.003	59	0.93	0.58
	3	Entropy+ MPP+ kurtosis	0.81±0.08	0.006	41	1.00	0.50
	4	Entropy+ MPP+ kurtosis	0.79±0.09	0.010	48	0.53	1.00
	5	Entropy+ MPP+ kurtosis	0.78±0.09	0.013	52	0.60	0.92
	6	Entropy+ MPP+ kurtosis[c]	0.84±0.08	0.077	52	0.67	1.00
CM	0	SD+ MPP+ skewness[c]	0.96±0.04	0.000	78	0.87	0.92
	2	Entropy+ MPP+ kurtosis	0.77±0.10	0.017	59	0.93	0.67
	3	Entropy+ MPP+ kurtosis	0.76±0.10	0.025	44	0.87	0.58
	4	Entropy+ MPP+ kurtosis	0.80±0.09	0.008	41	0.73	0.83
	5	SD+ entropy+ MPP	0.64±0.11	0.223	30	0.73	0.67
	6	SD+ entropy+ MPP	0.68±0.11	0.118	37	0.53	0.92
N	0	MPP+ skewness+ kurtosis[c]	0.93±0.05	0.000	70	0.93	0.83
	2	Entropy+ MPP+ skewness	0.74±0.10	0.032	37	0.93	0.50
	3	Entropy+ MPP+ skewness	0.78±0.09	0.013	44	0.60	1.00
	4	MPP+ skewness+ kurtosis	0.84±0.08	0.002	41	0.67	1.00
	5	Mean+ SD+ kurtosis	0.88±0.07	0.001	41	0.67	1.00
	6	SD+ entropy+ kurtosis	0.91±0.06	<0.001	63	0.87	0.92

RCC, renal cell carcinoma; pRCC, papillary RCC; chRCC, chromophobe RCC; AUC, area under the ROC curve; SSF, spatial scaling factor; SVM, support vector machine; Mean, mean grey-level intensity; SD, standard deviation; MPP, mean of positive pixels; UE, unenhanced; CM, corticomedullary; N, nephrographic.
[a] Data are mean AUC ± standard error.
[b] Accuracy of the SVM classifier after 10-fold cross-validation.
[c] Model with the highest AUC in each phase.

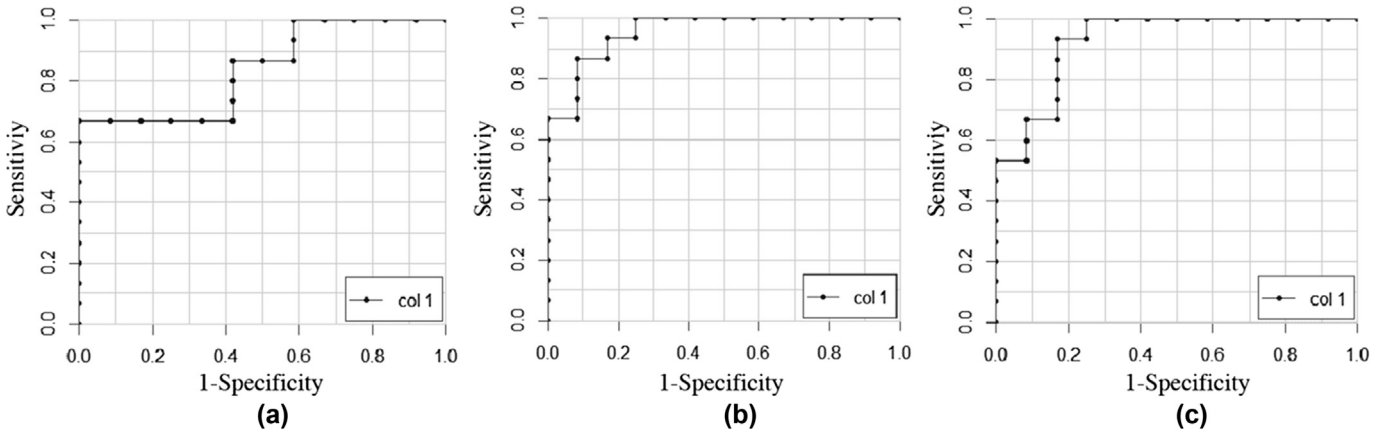

Figure 4 ROC curves for SVM performances with the highest AUC value for differentiating between pRCC and chRCC on (a) unenhanced, (b) corticomedullary, and (c) nephrographic phase images.

evaluating MRI images for classifying RCC subtypes, Chandarana *et al.*[28] found that kurtosis and skewness were significantly lower in ccRCC. Similar findings regarding kurtosis were found in the present study, but no difference in skewness was found among RCC subtypes. This could possibly be attributed to the differences between imaging techniques and physical properties being captured. The role of skewness on CT in discriminating RCC subtypes may need further investigation.

In the present study, both unenhanced and contrast-enhanced CT images were analysed. On unenhanced CT images, the results were slightly different from the results of previous studies. Hodgdon *et al.*[14] reported that there was no texture difference between RCC subtypes on unenhanced CT images. In the present study, individual texture parameters also showed no significant difference between RCC subtypes but combinations of different texture parameters could be used to help identify non-ccRCC from ccRCC and differentiate between pRCC and chRCC. One possible explanation could be combinations of texture parameters may help to enhance the detection of subtle, but potentially discriminating, features that individual parameters may not be able to reflect. Although the effects of iodinated contrast material on TA are still unclear, differences in texture features between unenhanced and contrast-enhanced CT images were observed in previous studies.[21,29] More texture parameters on enhanced images showed significant differences between RCC subtypes and models integrating texture parameters quantified from enhanced images demonstrated higher diagnostic accuracies. The present findings seem to support that CT TA on enhanced images may provide more useful information, specifically corticomedullary images, to identify non-ccRCC from ccRCC.

Before building the classifiers in the present study, Pearson's correlation coefficient between each feature was evaluated to make sure that the features selected to train SVM were not highly correlated. As an AUC of $\geq$0.8 generally indicates a good test, the optimal discriminative texture features were defined as those with an AUC of $\geq$0.8 and they were combined to train SVM at each SSF in each phase; however, there were some circumstances in which none of the texture parameters yielded an AUC of $\geq$0.8. In such situations and to minimise the likelihood of overfitting, the optimal discriminative texture features were selected as texture parameters with the top three AUC values; however, there are also other strategies to select and define SVM classifiers.[14,30] In the present study, most cross-validation accuracies for identifying non-ccRCC from ccRCC were $>$80% and some models resulted in 96% sensitivity and 92% specificity; however, when differentiating between pRCC and chRCC, cross-validation SVM accuracies were low (30–78%), but yet there was a model incorporating SD, MPP, and skewness quantified from SSF0 on corticomedullary images which produced an AUC of 0.96$\pm$0.04 ($p<0.001$) with 87% sensitivity and 92% specificity. The low cross-validation accuracy is likely related to the small sample size and it is possible that an increase in sample size would improve cross-validation accuracy. Larger cohorts of pRCC and chRCC are necessary to validate the present results.

The present study had several limitations. First, the retrospective nature of the study may lead to overestimation of the diagnostic accuracy. Second, although the sample size of non-ccRCC was comparable to that of previous studies involving differentiation of RCC subtypes by using CT TA, the small sample size may contribute to the low cross-validation accuracy. More data should be pooled to confirm the present results. Third, as 10 ccRCC that had almost no solid component were excluded, it is possible that texture characteristics of ccRCC reported in this study may not be comprehensive enough and the present results may not be generalised directly to those primarily cystic or necrotic lesions. Fourth, as the main purpose of this study was to investigate whether CT TA could be used to discriminate RCC subtypes, the correlation between texture parameters and histological grading within each subtype was not evaluated. The results of the present study add to clinical adoption of TA for evaluating RCC in addition to standard morphological assessment, which would give clinicians more confidence in making the optimal therapeutic choice for RCC patients.

In conclusion, the results of the present study show that CT TA could potentially be used to differentiate non-ccRCC

from ccRCC accurately, and further differentiate between pRCC and chRCC. Prospective studies in larger cohorts of patients are required to further validate these results before implementation in clinical practice.

Conflict of interest

The authors declare no conflict of interest.

Author contributions

1. guarantor of integrity of the entire study: H.S., Z.Y.J.
2. study concepts and design: H.S., G.M.Y.Z.
3. literature research: B.S., G.M.Y.Z.
4. clinical studies: H.D.X.
5. experimental studies/ data analysis: B.S., G.M.Y.Z.
6. statistical analysis: G.M.Y.Z, B.S.
7. manuscript preparation: G.M.Y.Z.
8. manuscript editing: G.M.Y.Z, H.S, B.G, Z.Y.J.

Acknowledgement

The authors thank Dr Wei Han and Dr Yuyan Wang from Department of Statistics, Peking Union Medical College for their professional statistical advice and assistance. This work was supported by grants from the Fundamental Research Funds for the Central Universities (grant no.: 3332018022 to S.H.) and the Education reform fund of Peking Union Medical College (grant no.:10023201700104 to S.H.).

Appendix A. Supplementary data

Supplementary data to this article can be found online at https://doi.org/10.1016/j.crad.2018.11.009.

References

1. Ljungberg B, Campbell SC, Choi HY, *et al.* The epidemiology of renal cell carcinoma. *Eur Urol* 2011;**20**:615–21.
2. Ljungberg B, Bensalah K, Canfield S, *et al.* EAU guidelines on renal cell carcinoma: 2014 update. *Eur Urol* 2015;**67**:913–24.
3. Patard JJ, Leray E, Rioux-Leclercq N, *et al.* Prognostic value of histologic subtypes in renal cell carcinoma: a multicenter experience. *J Clin Oncol* 2015;**23**:2763–71.
4. Capitanio U, Cloutier V, Zini L, *et al.* A critical assessment of the prognostic value of clear cell, papillary and chromophobe histological subtypes in renal cell carcinoma: a population-based study. *BJU Int* 2009;**103**:1496–500.
5. Hudes G, Carducci M, Tomczak P, *et al.* Temsirolimus, interferon alfa, or both for advanced renal-cell carcinoma. *N Engl J Med* 2007;**356**:2271–81.
6. Negrier S, Gravis G, Perol D, *et al.* Temsirolimus and bevacizumab, or sunitinib, or interferon alfa and bevacizumab for patients with advanced renal cell carcinoma (TORAVA): a randomised phase 2 trial. *Lancet Oncol* 2011;**12**:673–80.
7. Procopio G, Verzoni E, Bracarda S, *et al.* Italian Trials in Medical Oncology (ITMO) group. Overall survival for sorafenib plus interleukin-2 compared with sorafenib alone in metastatic renal cell carcinoma (mRCC): final results of the ROSORC trial. *Ann Oncol* 2013;**24**:2967–71.
8. Volpe A, Finelli A, Gill IS, *et al.* Rationale for percutaneous biopsy and histologic characterisation of renal tumours. *Eur Urol* 2012;**62**:491–504.
9. Young JR, Margolis D, Sauk S, *et al.* Clear cell renal cell carcinoma: discrimination from other renal cell carcinoma subtypes and oncocytoma at multiphasic multidetector CT. *Radiology* 2013;**267**:444–53.
10. Kim SH, Kim CS, Kim MJ, *et al.* Differentiation of clear cell renal cell carcinoma from other subtypes and fat-poor angiomyolipoma by use of quantitative enhancement measurement during three-phase MDCT. *AJR Am J Roentgenol* 2016;**206**:W21–8.
11. Cornelis F, Tricaud E, Lasserre AS, *et al.* Multiparametric magnetic resonance imaging for the differentiation of low and high grade clear cell renal carcinoma. *Eur Radiol* 2015;**25**:24–31.
12. Wang H, Cheng L, Zhang X, *et al.* Renal cell carcinoma: diffusion-weighted MR imaging for subtype differentiation at 3.0 T. *Radiology* 2010;**257**:135–43.
13. Yan L, Liu Z, Wang G, *et al.* Angiomyolipoma with minimal fat: differentiation from clear cell renal cell carcinoma and papillary renal cell carcinoma by texture analysis on CT images. *Acad Radiol* 2015;**22**:1115–21.
14. Hodgdon T, McInnes MD, Schieda N, *et al.* Can quantitative CT texture analysis be used to differentiate fat-poor renal angiomyolipoma from renal cell carcinoma on unenhanced CT images? *Radiology* 2015;**276**:787–96.
15. Kim TY, Choi HJ, Hwang HG, *et al.* Three-dimensional texture analysis of renal cell carcinoma cell nuclei for computerized automatic grading. *J Med Syst* 2010;**34**:709–16.
16. Raman SP, Chen Y, Schroeder JL, *et al.* CT texture analysis of renal masses: pilot study using random forest classification for prediction of pathology. *Acad Radiol* 2014;**21**:1587–96.
17. Miles KA, Ganeshan B, Hayball MP. CT texture analysis using the filtration-histogram method: what do the measurements mean? *Cancer Imag* 2013;**13**:400–6.
18. Cross EM, Chaffin WW. Use of the binomial theorem in interpreting results of multiple tests of significance. *Educ Psychol Meas* 1982;**42**:25–34.
19. Chang C, Lin C. LIBSVM: a library for support vector machines. *ACM Trans Intell Syst Technol* 2011;**2**:1–27.
20. Goh V, Ganeshan B, Nathan P, *et al.* Assessment of response to tyrosine kinase inhibitors in metastatic renal cell cancer: CT texture as a predictive biomarker. *Radiology* 2011;**261**:65–171.
21. Ganeshan B, Goh V, Mandeville HC, *et al.* Non-small cell lung cancer: histopathologic correlates for texture parameters at CT. *Radiology* 2013;**266**:326–36.
22. Ganeshan B, Panayiotou E, Burnand K, *et al.* Tumour heterogeneity in non-small cell lung carcinoma assessed by CT texture analysis: a potential marker of survival. *Eur Radiol* 2012;**22**:796–802.
23. Andersen MB, Harders SW, Ganeshan B, *et al.* CT texture analysis can help differentiate between malignant and benign lymph nodes in the mediastinum in patients suspected for lung cancer. *Acta Radiol* 2016;**57**:669–76.
24. Li Z, Mao Y, Li H, *et al.* Differentiating brain metastases from different pathological types of lung cancers using texture analysis of T1 post-contrast MR. *Magn Reson Med* 2016;**76**:1410–9.
25. Smith AD, Gray MR, del Campo SM, *et al.* Predicting overall survival in patients with metastatic melanoma on antiangiogenic therapy and RECIST stable disease on initial posttherapy images using CT texture analysis. *AJR Am J Roentgenol* 2015;**205**:W283–93.
26. De Cecco CN, Ganeshan B, Ciolina M, *et al.* Texture analysis as imaging biomarker of tumoural response to neoadjuvant chemoradiotherapy in rectal cancer patients studied with 3-T magnetic resonance. *Invest Radiol* 2015;**50**:239–45.
27. Tian F, Hayano K, Kambadakone AR, *et al.* Response assessment to neoadjuvant therapy in soft tissue sarcomas: using CT texture analysis in comparison to tumour size, density, and perfusion. *Abdom Imag* 2015;**40**:1705–12.
28. Chandarana H, Rosenkrantz AB, Mussi TC, *et al.* Histogram analysis of whole-lesion enhancement in differentiating clear cell from papillary subtype of renal cell cancer. *Radiology* 2012;**265**:790–8.
29. Ng F, Ganeshan B, Kozarski R, *et al.* Assessment of primary colorectal cancer heterogeneity by using whole-tumour texture analysis: contrast-enhanced CT texture as a biomarker of 5-year survival. *Radiology* 2013;**266**:177–84.
30. Ng F, Kozarski R, Ganeshan B, *et al.* Assessment of tumour heterogeneity by CT texture analysis: can the largest cross-sectional area be used as an alternative to whole tumour analysis? *Eur J Radiol* 2013;**82**:342–8.